Songklanakarin J. Sci. Technol.
39 (4), 489-496, Jul - Aug. 2017

http://www.sjst.psu.ac.th

Original Article

Numerical modeling of combustion of low-calorific-producer-gas from Mangium wood within a late mixing porous burner (LMPB)

Kanokkarn Jirakulsomchok[1,2]* and Kampanart Theinnoi[1,2]

[1] *College of Industrial Technology, King Mongkut's University of Technology North Bangkok, Bang Sue, Bangkok, 10800 Thailand*

[2] *Research Centre for Combustion Technology and Alternative Energy (CTAE), Science and Technology Research Institute, King Mongkut's University of Technology North Bangkok, Bang Sue, Bangkok, 10800 Thailand*

Received: 14 January 2016; Revised: 25 May 2016; Accepted: 12 July 2016

Abstract

This article presents a numerical study of combustion of low-calorific-producer-gas from Mangium wood within a late mixing porous burner (LMPB). The LMPB consists of four main components, i.e., the fuel preheating porous (FP), the porous combustor (PC), the air jacket, and the mixing chamber. Interestingly, this LMPB was able to highly preheated and it still maintained high safety in operation. A single-step global reaction, steady state approach and a one-dimensional model were considered. The necessary information for burner characteristics, i.e., temperature profile, flame location and maximum temperature were also presented. The results indicated that stable combustion of a low-calorific-producer-gas within LMPB was possible achieved. Increasing equivalence ratio resulted in increasing in the flame temperature. Meanwhile, increasing the firing rate caused slightly decrease in flame temperature. The flame moved to downstream zone of the PC when the firing rate increased. Finally, it was found that the equivalence ratio did not affect the flame location.

Keywords: porous, combustion, biomass gasification, producer gas, low-calorific-producer-gas

1. Introduction

In the past decades, there is a wide interest in biomass fuel due to the advantage of its lower emission of carbon dioxide and other greenhouse gases. Biomass means all organic materials are originated from living, or recently living organisms. In the developing countries, biomass is used as fuel for cooking and heating. Among all biomass utilization, the conversion process by gasification is one of the promising ones. The biomass gasification process provides higher energy efficiency than that of combustion Devi *et al.* (2003). Producer gas from gasification process is composed of the combustible gas (i.e. CO, H_2, CH_4) and the inert content (CO_2 and N_2). Typical producer gas from biomass gasification emits high concentration of inert gas over 50% by volume. The high inert content reduces the flame temperature and the burning velocity. As a result the stabilization combustion difficultly occurs.

The flame embedded within the porous burner provides higher burning velocity and leaner flammability limits than conventional open flames. This is due to the internal heat recirculating from the hot product gas at the post flame zone to the fresh mixture at the pre-flame zone by the combination of conduction, convection and radiation heat transfer without an external heat exchanger. In other words, the porous medium acts as a heat exchanger. Similar to a premixed flame, within the porous burner is divided into two zones, the preheat zone and the reaction zone. The

* Corresponding author.
Email address: kanokkarn.j@cit.kmutnb.ac.th

preheat zone begins where the fresh mixture temperature has increased by 1% of its original inlet value and end there the gas and solid temperature are equal. Reactant preheating in the porous burner occurs due to solid-to-solid conduction and solid-to-solid radiation. The dominant mode of heat recirculation depends on, equivalence ratio and flame speed ratio. Increasing equivalence ratio and flame speed, radiative heat transfer becomes the dominant mode of heat recirculation. This results in a decrease of the solid-to-gas convective in the preheat zone and the heat recirculation efficiency (Barra & Ellzey, 2004). Many articles review research that has explored combustion in porous media (Howell *et al.*, 1996; Mujeebu *et al.*, 2009a, 2009b; Trimis & Durst, 1996; Wood & Harris, 2008).

Numerous studies have focused on combustion of simulated low calorific gases from landfills, biogas, natural gas and waste pyrolysis within two-layer porous burners. The results indicated that the inert species in the gas mixture reduce the adiabatic flame temperature and the burning velocity depending on its heat capacity (Al-Hamamre *et al.*, 2006). At near stoichiometric regimes, the flame temperature reaches 1,500 K and decrease below 1,200 K with increasing excess air ratio at low firing rate. The porous burner can be operated at a wide range of firing rate with low emission both NOx and CO, i.e. less than 50 ppm (Alavandi & Agrawal, 2008; Keramiotis *et al.*, 2015). However, the previous work focused on premixed flame within two-layer porous burner, which is low safety and having only single preheat zone (i.e. in the first porous section).

Wongwatcharaphon *et al.* (2009, 2013) propose a new concept of late mixing porous burner that provides highly preheating effect with safety in operation. The fuel and air supplies are separated for a non-premixed flame mode propose. The fuel preheating zone in the upstream porous, the air preheating zone in the air jacket, and the mixture preheating zone in the downstream porous. The fuel, air, and mixture are preheated before combustion occurs. This results in high heat recirculation and radiant output. Moreover, the LMPB is a fuel-flexible burner can be used for gaseous or liquid fuel in the same burner. However, the combustion of low-calorific-producer-gas from biomass gasification process has not been studied.

In this paper, the study of combustion of a low-ccalorific-producer-gas from biomass gasification within a late mixing porous burner (LMPB) was studied. Mangium (also known as krathin-thepha) is used as raw material for gasification because it is fast-growing tree and can be planted in every provinces of Thailand. Moreover, its cost is low. A single-step global reaction model, steady state approach and a one-dimensional model were assumed. The numerical model is presented to predict gas and solid temperature under a variety of operating conditions. The temperature profile, the maximum temperature, and the flame location are reported, which can be used as a guide line for future experimental study.

2. Numerical Model

The geometry of LMPB is shown in Figure 1. The LMPB consists of two porous inert media. The upstream porous is the fuel preheating porous (FP), use to fuel preheated. The downstream porous is the porous combustor (PC) which is surrounded by the air jacket. The FP and the PC are coupled by thermal radiation emitted from the PC to

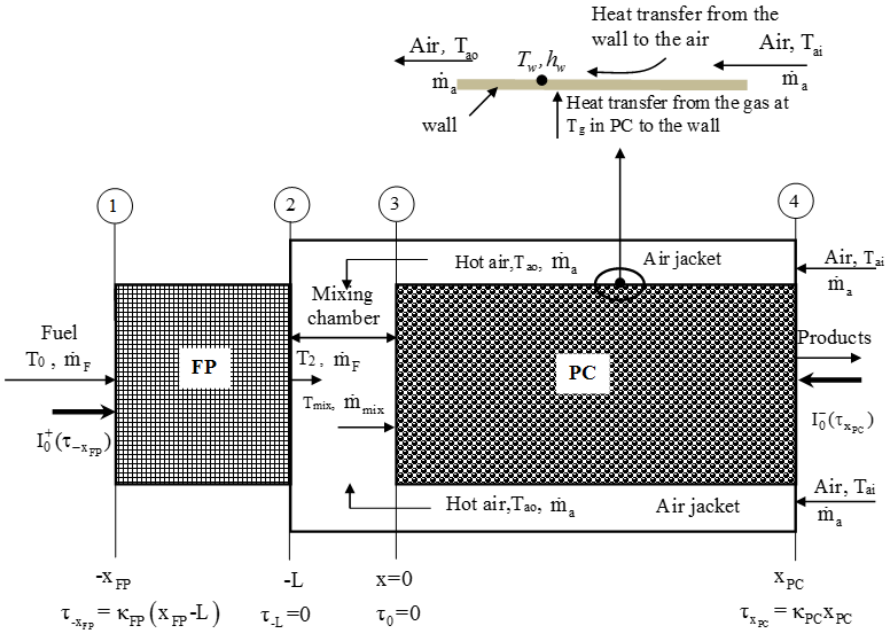

Figure 1. Burner geometry.

the FP for preheating low-calorific-producer-gas. The FP is a stack of metallic wire screens are installed inside a stainless steel tube of 75 mm in length. The PC is a packed bed of alumina ball with a diameter of 10 mm randomly packed inside the 160 mm (in length) of stainless steel tube. The diameter both FP and PC are 60 mm. At steady state condition, the producer gas at T_0 flows into the FP at section 1 and is preheated in porous FP. At once, the air at T_{ai} flows through an annular air jacket at section 4, and is preheated by the hot wall of PC. The preheated fuel from section 2 and the preheated air flow out from section 3 meet and mix together in the mixing chamber. The homogeneous mixture of hot fuel and the hot air at T_{mix} flow through the PC and is burned. The solid and gas phase conduction, solid radiation, and heat transfer between the solid and gas phase are also considered in the numerical model. Both ends of the LMPB are exposed to black surroundings maintained at ambient temperature T_0, providing incident radiation $I_0^+\left(\tau_{-x_{FP}}\right)$ at section 1 and $I_0^-\left(\tau_{x_{PC}}\right)$ at section 4, respectively. By the concept of three preheating zone, the LMPB can allow for a stable combustion of low calorific producer gas.

The gas and solid phase energy equation both in FP and PC were solved for analyzing combustion and heat transfer process. A single-step global reaction model, steady state approach and a one dimensional model are considered. The conservation equation of species and energy both in FP and PC are discretized by finite differential approximations. An implicit difference scheme is adopted with respect to time, and a central difference scheme is adopted with respect of space. The convergence criteria of all variables for numerical computation are set to 10^{-6}. The final error in the energy balance is usually less than 1%.

The principal assumptions used in the model are as follows:

(a) Flow and heat transfer are one-dimensional and in steady state.

(b) Working gas is non-radiating and behaves as ideal gases.

(c) FP and PC are able to emit and absorb thermal radiation in local thermal equilibrium, while radiative scattering is ignored.

(d) The flow is incompressible, because the flow velocity is very small when compared to the sound speed.

(e) The heat and mass simultaneously transfer by convection, then Lewis number is unity.

(f) The physical properties are constant i.e. specific heat, porosity, absorption coefficient, thermal conductivity, and density.

(g) Good thermal insulation system. In other words, the system undergoes an adiabatic process.

(h) Porous media are inert both in FP and PC.

(i) In FP, the mechanisms of hydrocarbon thermal cracking are negligible.

(j) The fuel/air mixture at temperature T_{mix} is completely premixed as it enters the PC at section 3.

(k) The combustion reaction is described by an irreversible first-order reaction: Reactants $\rightarrow$ Products.

(l) Based on the experimental results, peak temperatures are observed within the region of the PC. This indicates that main combustion is taken place inside the PC. Thus, reaction is assumed to start and get completed only in the PC.

(m) The PC wall temperature at T_w is constant because of good thermal conductivity of the wall.

2.1 Basic equations

The governing equations are as follows.

In the FP section, $-x_{FP} \le x \le -L$ $\left(\tau_{-x_{FP}} \le \tau \le \tau_{-L}\right)$, the conservation equations for energy of gas and solid phase are given by

$$\rho_F c_F \varepsilon_{FP} \frac{\partial T_F}{\partial t} + \rho_F u_F c_F \varepsilon_{FP} \frac{\partial T_F}{\partial x} = \lambda_F \varepsilon_{FP} \frac{\partial^2 T_F}{\partial x^2} - h_v (T_F - T_s),$$

and (1)

$$\rho_s c_s \left(1-\varepsilon_{FP}\right) \frac{\partial T_s}{\partial t} = \lambda_e \frac{\partial^2 T_s}{\partial x^2} - \frac{\partial q_r^n}{\partial x} + h_v (T_F - T_s). \quad (2)$$

where the local net radiative heat flux within the FP is expressed as: $q_r^n(\tau) = q_r^+(\tau) + q_r^-(\tau)$,

$$q_r^+(\tau) = 2\pi\left[I_0^+(\tau_{-x_{FP}}) E_3\left(\tau_{-x_{FP}} - \tau\right) + \int_{\tau_{-x_{FP}}}^{\tau} I_b(\tau') E_2(\tau' - \tau)\, d\tau \right],$$

and (3)

$$q_r^-(\tau) = -2\pi\left[I_0^-(\tau_{x_{PC}}) E_3\left(\tau_{x_{PC}}\right) + \int_0^{\tau_{x_{PC}}} I_b(\tau') E_2(\tau')\, d\tau' \right] E_3(\tau)$$

$$-2\pi\left[\int_{\tau}^{\tau_{-L}} I_b(\tau') E_2(\tau - \tau')\, d\tau' \right]. \quad (4)$$

The optical thickness in the FP section is defined as $\tau = \kappa_{FP}(-L - x)$. The divergence of net radiative heat flux, $\frac{\partial q_r^n(\tau)}{\partial x}$ in Equation (2), is evaluated from the integration of the radiant flux from each part of the porous media FP and PC, and is expressed as:

$$\frac{\partial q_r^n(\tau)}{\partial x} =$$

$$-2\kappa_{FP}\pi\left[-2I_b(\tau) + \int_{\tau_{-x_{FP}}}^{\tau_{-L}} I_b(\tau') E_1\left(|\tau - \tau'|\right) d\tau' + I_0^+\left(\tau_{-x_{FP}}\right) E_2\left(\tau_{-x_{FP}} - \tau\right) \right]$$

$$-2\kappa_{FP}\pi\left[I_0^-\left(\tau_{x_{PC}}\right) E_3\left(\tau_{x_{PC}}\right) + \int_0^{\tau_{x_{PC}}} I_b(\tau') E_2(\tau')\, d\tau' \right] E_2(\tau). \quad (5)$$

where $I_b(\tau)=\dfrac{\sigma T_s^4(\tau)}{\pi}$,

and $E_n(\tau)=\int_0^1 \eta^{n-2}e^{-\tau/\eta}d\eta,\ n=1,2,3.$

In the mixing chamber, the conservation equations for mass and energy are given by

$$\dot{m}_{mix}=\dot{m}_F+\dot{m}_a, \text{ and} \tag{6}$$

$$\dot{m}_{mix}h_{mix}(T_{mix})=\dot{m}_F h_F(T_2)+\dot{m}_a h_a(T_{ao}). \tag{7}$$

In the PC section, $0\le x\le x_{PC}$ $\left(\tau_0\le\tau\le\tau_{x_{PC}}\right)$

Gas phase energy equation:

$$\rho_g c_g \varepsilon_{PC}\frac{\partial T_g}{\partial t}+\rho_g u_g c_g \varepsilon_{PC}\frac{\partial T_g}{\partial x}=$$

$$\lambda_g \varepsilon_{PC}\frac{\partial^2 T_g}{\partial x^2}+\varepsilon_{PC}h_o w-h_v(T_g-T_s)-\alpha U_w(T_g-T_w). \tag{8}$$

The last term on the right-hand side of Equation (8) is heat transfer from the hot gas in PC to the wall, which preheats the air flowing in the air jacket. The reaction rate is considered to follow the first-order Arrhenius equation,

$$w=A\rho(1-y)e^{-E/RT}. \tag{9}$$

The conservation equation for the species of gas phase in PC is given by

$$\rho_g \varepsilon_{PC}\frac{\partial y}{\partial t}+\rho_g u_g \varepsilon_{PC}\frac{\partial y}{\partial x}=D\rho_g \varepsilon_{PC}\frac{\partial^2 y}{\partial x^2}+\varepsilon_{PC}w. \tag{10}$$

Solid phase energy equation:

$$\rho_s c_s(1-\varepsilon_{PC})\frac{\partial T_s}{\partial t}=\lambda_e\frac{\partial^2 T_s}{\partial x^2}-\frac{\partial q_r^n}{\partial x}+h_v(T_g-T_s). \tag{11}$$

Where the local net radiative heat flux within the PC is expressed as: $q_r^{\,n}(\tau)=q_r^{\,+}(\tau)+q_r^{\,-}(\tau)$,

$$q_r^{\,+}(\tau)=2\pi\left[I_0^+(\tau_{-x_{FP}})E_3(\tau_{-x_{FP}})+\int_{\tau_{-x_{FP}}}^{\tau_{-L}} I_b(\tau')E_2(\tau')d\tau'\right]E_3(\tau)$$

$$+2\pi\left[\int_0^{\tau} I_b(\tau')E_2(\tau-\tau')\,d\tau'\right], \text{ and} \tag{12}$$

$$q_r^{\,-}(\tau)=-2\pi\left[I_0^-(\tau_{x_{PC}})E_3(\tau_{x_{PC}}-\tau)+\int_{\tau}^{\tau_{x_{PC}}} I_b(\tau')E_2(\tau'-\tau)d\tau'\right]. \tag{13}$$

The optical thickness in the PC section is defined as $\tau=\kappa_{PC}(x)$. The divergence of the net radiative heat flux, $\dfrac{\partial q_r^n(\tau)}{\partial x}$ in Equation (11), is expressed as:

$$\frac{\partial q_r^n(\tau)}{\partial x}=$$

$$-2\pi\kappa_{PC}\left[I_0^+(\tau_{-x_{FP}})E_3(\tau_{-x_{FP}})+\int_{\tau_{-x_{FP}}}^{\tau_{-L}} I_b(\tau')E_2(\tau')d\tau'\right]E_2(\tau)$$

$$-2\pi\kappa_{PC}\left[-2I_b(\tau)+I_0^-(\tau_{x_{PC}})E_2(\tau_{x_{PC}}-\tau)+\int_0^{\tau_{x_{PC}}} I_b(\tau')E_1(|\tau-\tau'|)d\tau'\right], \tag{14}$$

where the last term of the Equation (14) is defined as

$$\int_0^{\tau_{x_{PC}}} I_b(\tau')E_1(|\tau-\tau'|)d\tau'=$$

$$\int_0^{\tau} I_b(\tau')E_1(\tau-\tau')\,d\tau'+\int_{\tau}^{\tau_{x_{PC}}} I_b(\tau')E_1(\tau'-\tau)d\tau'.$$

There are nine unknowns, T_F and T_s in the FP: $\dot{m}_{mix}$, T_{mix} and T_{ao} in the mixing chamber, T_g, T_s, y and T_w in the PC, but there are seven equations to be solved. Thus, another two equations are needed in the air jacket, which are shown in Equation (15) and (16).

In the air jacket (see Figure 1), heat transfer from the hot gas in PC to the wall is equal to heat convection from the wall to the combustion air in the air jacket, which is equal to an increase in the sensible heat of the combustion air flowing in the air jacket. Therefore, we obtain

$$\int_0^{x_{PC}} U_w(T_g-T_w)(2\pi r_{PC})\,dx=h_w A_w \Delta T_{ln}, \tag{15}$$

$$\dot{m}_a c_a dT_a=h_w(T_w-T_a)dA, \tag{16}$$

where $\Delta T_{ln}=\dfrac{T_{ai}-T_{ao}}{\ln\left[\dfrac{T_w-T_{ao}}{T_w-T_{ai}}\right]}$ and the air inlet temperature T_{ai} is considered to be equal to ambient temperature.

T_{ao}, in terms of T_w and T_{ai}, can be determined by integrating Equation (16) over the surface area of the wall. By substituting T_{ao} into Equation (15) gives the following equation, $T_w=\dfrac{C\int_0^{x_{PC}} T_g(x)dx+(B-1)T_{ai}}{D}$, where B, C, and D are defined as $B=\exp(-2\pi r_{PC}x_{PC}h_w/\dot{m}_a c_a)$, $C=2\pi r_{PC}U_w \ln B/(h_w A_w)$ and $D=C+Bx_{PC}-1$.

Since the fuel flow rate in the FP is small compared with the combustion air, the heat transfer between the gas and solid phases is not significantly changed with varying firing rates. Thus, the volumetric heat transfer Yoshizawa *et al.* (1988) in FP is considered constant and is equal to 9.1×10^5 W/m^{3}K. The correlation for volumetric heat transfer coefficient Nu_v used in PC is given by the following correlation Wakao *et al.* (1979):

$$Nu_v = h_v d_p^2 / \lambda_g = A_{sf} d_P \left(2 + 1.1 Re_{d_P}^{0.6} Pr^{1/3}\right), \quad (17)$$

where the specific surface area is defined as $A_{sf} = \frac{6(1-\varepsilon_{PC})}{d_P}$.

Because the porous structure of PC is a packed bed of randomly arranged spheres, the effective thermal conductivity is difficult to estimate. This work uses the relation $\lambda_e = (1-\varepsilon_{PC})\lambda_s$ when continuous structure of the PC is assumed. The convergence criteria for numerical computation of all variables are set to 10^{-6}.

The heat transfer phenomena at the FP exit (x = -L) and at the PC inlet (x = 0) boundary are very complicated, because of combination of radiation between the two porous media of FP and PC, convection between high swirling air and porous ends, and gas conduction. However, from preliminary calculation, we found that zero heat flux boundary condition was suitable for the model because this provides the nearest result with the experimental ones. The boundary conditions are summarized in Table 1. The initial conditions for these simulations are obtained from experimental data. The physical properties of gas, based on the average temperature at each zone of FP, a mixing chamber and PC, are constant. All the properties used are summarized in Table 2. The conservation equations of species and energy both in FP and PC are discretized by finite differential approximations. An implicit difference scheme is adopted with respect to time, and a central difference scheme is adopted with respect to space.

3. Results and Discussion

3.1 Gas composition

Figure 2 shows the average compositions of producer gas from Mangium wood that is based on our previous experiment. The gas chromatography is used to measure the gas composition. The producer gas is mixture of 14.66% H_2, 10.50% CH_4, 9.54% CO, 13.33% CO_2, and 51.97% N_2. The experimental result indicated that the producer gas has high inert content of CO_2 and N_2. Therefore, the average calculated heating value of producer gas is low, 5842 kJ/kg.

Table 1. Boundary conditions.

FP Section		PC Section	
$x = -x_{FP}$	$x = -L$	$x = 0$	$x = x_{PC}$
$T_F = T_0$	$\frac{\partial T_F}{\partial x} = 0$	$T_g = T_{mix}$	$\frac{\partial T_g}{\partial x} = 0$
$\frac{\partial T_s}{\partial x} = 0$	$\frac{\partial T_s}{\partial x} = 0$	$\frac{\partial T_s}{\partial x} = 0$	$\frac{\partial T_s}{\partial x} = 0$
-	-	$y = y_0$	$\frac{\partial y}{\partial x} = 0$
$I_0^+(\tau_{-x_{FP}}) = \frac{\sigma T_0^4}{\pi}$	$I^-(\tau_{-L}) = I_0^-(\tau_{x_{PC}}) E_3(\tau_{x_{PC}}) + \int_0^{\tau_{x_{PC}}} I_b(\tau') E_2(\tau') d\tau'$	$I^+(\tau_0) = I_0^+(\tau_{-x_{FP}}) E_3(\tau_{-x_{FP}}) + \int_{\tau_{-x_{FP}}}^{\tau_{-L}} I_b(\tau') E_2(\tau') d\tau'$	$I_0^-(\tau_{x_{PC}}) = \frac{\sigma T_0^4}{\pi}$

Table 2. Solid property data used for simulations.

Properties	FP	PC	Unit
Porosity, ε	0.61	0.36	-
Effective thermal conductivity of solid, λ_e	12.1	1.8	$W.m^{-1}.K^{-1}$
Volumetric heat transfer coefficient, h_v	Yoshizawa *et al. (*1988*)*	Wakao *et al. (*1979*)*	$W.m^{-3}.K^{-1}$
Absorption coefficient, κ	1750	71	m^{-1}
Apparent density, $\rho_s(1-\varepsilon)$	2510	1714	kg/m^3
Specific heat, c_s	3120	775	$J.kg^{-1}.K^{-1}$

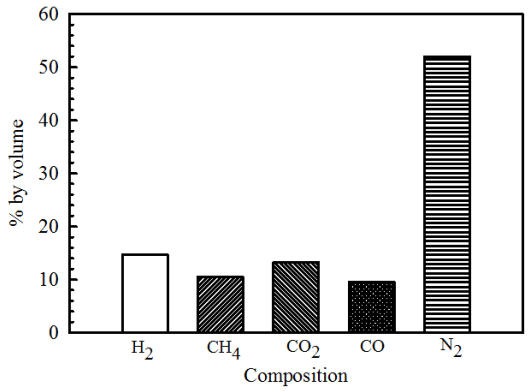

Figure 2. Dry producer gas compositions.

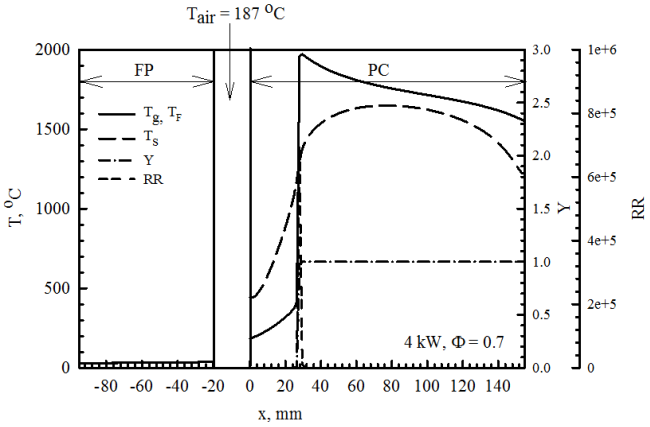

Figure 3. Temperature profile.

3.2 Temperature profile and radiative heat flux

Figure 3 shows the fuel temperature (T_F), gas temperature (T_g), solid temperature (T_s), product mole fraction (Y), and dimensionless reaction rate (RR) at equivalence ration (F) of 0.7 and firing rate (FR) of 4 kW. The FP and PC are coupled with thermal radiation. The FP act as a radiative heat absorber while the PC is heat emitter respectively. Considering in the FP, the solid temperature is slightly higher than the gas temperature and are nearly identical because of a high heat transfer between the gas and solid phases. A combustion air is preheated by the hot wall of the PC and flow into the mixing chamber with temperature of 187°C before mixing with the producer gas followed by combustion in the PC. In the PC, at the pre-flame zone, the solid temperature is higher than the gas phase temperature thus heat is transferred from the solid to the gas phase. In the reaction zone, high heat release from combustion process lead to maximum gas temperature that indicate the flame zone. At the post flame zone, the gas temperature is higher than solid temperature; therefore, heat is transferred from the gas to the porous structure. Suddenly, the heat recirculation by solid to solid conduction and radiation from the post-flame zone to the pre-flame zone occur. Then, the gas mixture flow through the PC is preheated before burnt in the flame zone. This result in the excess enthalpy flame occurs. This indicated that the LMPB can be used to burn the low-calorific-producer-gas and provide stabilizes combustion within porous medium. The global energy balance calculation has a small error (<1%). Moreover, the numerical result shows the same trend as previous work (Wongwatcharaphon *et al.*, 2009, 2013) and the same phenomenon as that of normal premixed porous burner (Bara & Ellzey, 2004; Diamantis *et al.*, 2002; Panigrahy & Mishar, 2016; Yoshizawa *et al.*, 1988b).

Figure 4 shows the radiative heat flux at 4 kW and $\Phi = 0.7$. The H^n mean net radiative heat flux, which is summation of radiative heat flux direction from left to right and the radiative heat flux direction from right to left. In PC, at the pre-flame zone heat is radiated from the reaction zone to the upstream end, then heat is radiated from porous PC to FP (negative H^n). In FP, heat is radiated from the hot zone (downstream zone) to the cooler zone (upstream zone), thus the H^n is negative near the end of downstream. While at the post-flame zone of PC, heat is radiated from the reaction zone to the downstream zone (positive H^n).

3.3 Effect of equivalence ratio

Figure 5 shows the effect of equivalence ratio on the gas temperature in the range of $\Phi = 0.6$-1 at firing rate of 4 kW. In this work, increasing Φ at a fixed firing rate, the air flow rate is decreased. Increasing Φ leads to an increase in quality of mixture and decrease in flow velocity (decrease in convective heat loss at the downstream zone). The graph shows that increasing Φ result in increasing flame temperature in PC, while F does not affect flame location.

3.4 Effect of firing rate

Figure 6 shows the effect of firing rate on the gas temperature in the range of FR = 1-5 kW at equivalence ratio of 0.7. Increasing FR cause to the flame move to the

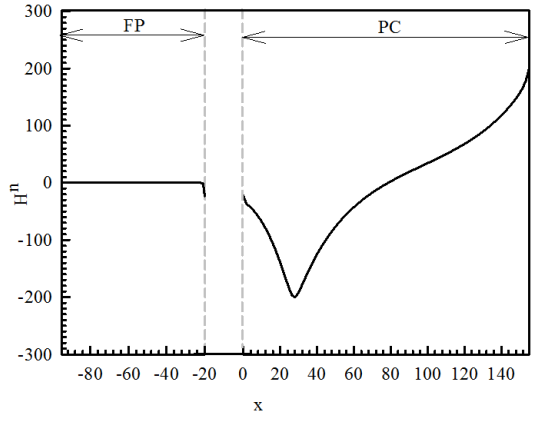

Figure 4. the radiative heat flux.

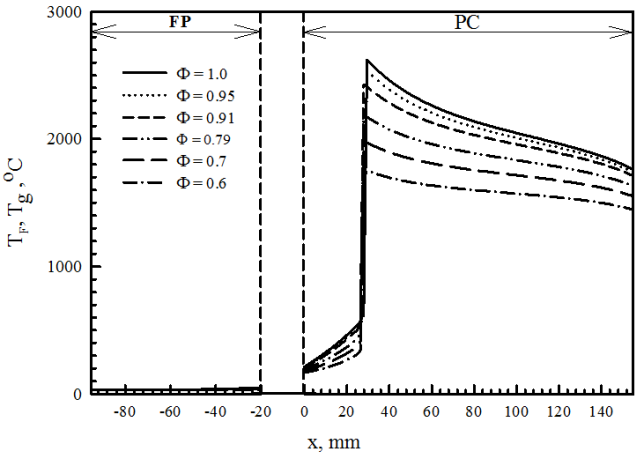

Figure 5. Effect of equivalence ratio on the gas temperature

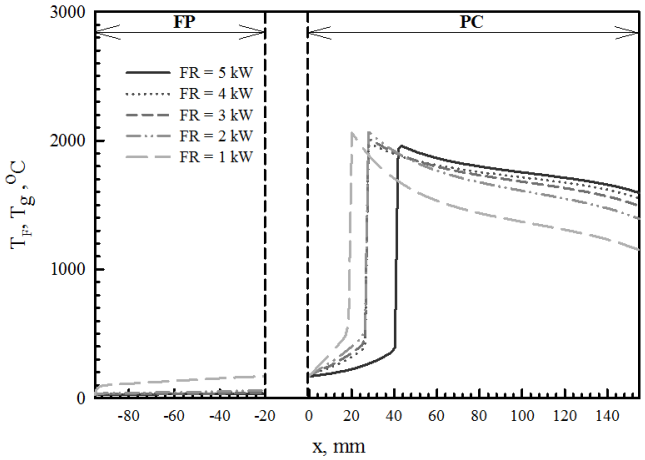

Figure 6. Effect of firing rate on the gas temperature

downstream zone of PC. The maximum temperature slightly decreases while the temperature at the post-flame zone increases; because more convective heat transfers from the flame zone to the downstream when FR increases. Moreover, the heat radiation to the FP decreases with flame moving to the downstream zone.

4. Conclusions

This paper proposes a one-dimensional numerical modeling for combustion of a low-calorific-producer-gas from Mangium wood within a late mixing porous burner (LMPB). The numerical results provide necessary information for burner characteristics, i.e., temperature profile, flame location and maximum temperature. The equivalence ratio and firing rate are important parameters affect thermal structure of the LMPB. The conclusions are as follow:

1. Increasing equivalence ratio, result in increasing in the flame temperature in PC, while equivalence ratio does not affect flame location.

2. Increasing FR cause to the flame move to the downstream zone of PC. The maximum temperature slightly decreases while the temperature at the post-flame zone increases.

The LMPB is a one possible technology for a low-calorific-producer-gas from gasification process because of highly three preheat zone: the fuel preheat zone in the FP, the air preheat zone in the air jacket and the mixture preheat zone in the pre-flame zone of the PC.

Nomenclature

A = area (m^2), frequency factor of combustion (s^{-1})
B = dummy variable
c = specific heat (J/kg.K)
C = dummy variable
FR = firing rate (kW)
d_p = diameter of particle (m)
D = diffusion coefficient (m^2/s), dummy variable
E = activation energy (kJ/mol)
E_n = exponential integral function
h = enthalpy (J/kg)
h_o = heat of reaction (J/m^3)
h_v = volumetric heat transfer coefficient ($W/m^3.K$)
H = local net radiative heat flux (-)
I = incident radiation (W/m^2)
L = length of mixing chamber (m)
$\dot{m}$ = mass flow rate (kg/s)
Nu = Nusselt number
Pr = Prandtl number
q_r = radiation flux (W/m^2)
r = radius (m)
R = gas constant (J/mol.K)
Re = Reynolds number
t = time (s)
T = temperature (K, °C)
u = interstitial gas velocity (m/s)
U = overall heat transfer coefficient ($W/m^2.K$)
V = volume (m^3)
w = reaction rate (1/s)
x = coordinate system (m)
y = product mole fraction
α = wall area to volume ratio (m^2/m^3)
ε = porosity
κ = absorption coefficient (m^{-1})
λ = thermal conductivity (W/m.K)
λ_e = effective thermal conductivity (W/m.K)
ρ = density (kg/m^3)
σ = Stefan – Boltzmann constant ($W/m^2.K^4$)
τ = optical thickness = κ x

Superscripts

\+ = positive direction
\- = negative direction
n = net

Subscripts

0 = ambient
a = air
ai = air inlet of air jacket
ao = air outlet of air jacket
ad = adiabatic
b = black body
F = fuel
FP = fuel-preheating porous medium
g = gas
mix = mixture
v = volumetric
w = wall
p = particle
PC = porous combustor
s = solid

Acknowledgements

This research was funded by the College of Industrial Technology, King Mongkut's University of Technology North Bangkok.

References

Alavandi, S. K., & Agrawal, A. K. (2008). Experimental study of combustion of hydrogen-syngas/methane fuel mixtures in a porous burner. *Hydrogen Energy, 33*, 1407-1415.

Al-Hamamre, Z., Diezinger, S., Talukdar, R, Von Isendorff, F., & Trimis, D. (2006). Combustion of low calorific gases from landfills and waste pyrolysis using porous medium burner technology. *Institution of Chemical Engineers, 84*(B4), 297-308.

Barra, A. J., & Ellzey, J. L. (2004). Heat recirculation and heat transfer in porous burners. *Combustion and Flame, 137*, 230-241.

Devi, L., Ptasinski, K. J., & Janssen, F. J. J. G. (2003). A review of the primary measures for tar elimination in biomass gasification processes. *Biomass and Bioenergy. 24*, 125-140.

Diamantis, D. J., Mastorakos, E., & Goussis, D. A. (2002). Simulations of premixed combustion in porous media. *Combustion Theory and Modelling, 6*, 383-411.

Howell, J. R., Hall, M. J., & Ellzey, J .L. (1996). Combustion of hydrocarbon fuels within porous inert media. *Progress in Energy and Combustion Science, 22*, 121-145.

Keramiotis, C., Katoufa, M., Vourliotakis, G., Hatziapostolou, A., & Founti, M. A. (2015). Experimental investigation of a radiant porous burner performance with simulated natural gas, biogas and synthesis gas fuel blends. *Fuel, 158*, 835-842.

Mujeebu, M. A., Abdullah, M. Z., Abu Bakar, M. Z., Mohamad, A. A., & Abdullah, M. K. (2009a). Applications of porous media combustion technology – A review. *Applied Energy, 86*, 1365-1375.

Mujeebu, M. A., Abdullah, M. Z., Abu Bakar, M. Z., Mohamad, A. A., & Abdullah, M. K. (2009b). A review of investigations on liquid fuel combustion in porous inert media. *Progress in Energy and Combustion Science, 35*(2), 216-230.

Panigrahy, S., & Mishar, C. S. (2016). Analysis of combustion of liquefied petroleum gas in a porous radiant burner. *International Journal of Heat and Mass Transfer, 95*, 488-498.

Trimis, D., & Durst, F. (1996). Combustion in a porous media: Advance and applications. *Combustion Science and Technology, 121*, 13-168.

Wakao, N., Kaguei, S., & Funazkri, T. (1979). Effect of fluid dispersion coefficients on particle-to fluid heat transfer coefficients in packed beds: Correlation of Nusselt numbers. *Chemical Engineering Science, 34*, 325-336.

Wongwatcharaphon, K., Tongtem, P., & Jugjai, S. (2009). Highly preheated fuel and air in nonpremixed porous burner. *Proceeding of the World Renewable Energy Congress 2009 – Asia The 3rd International Conference on "Sustainable Energy and Environment (SEE 2009)*" (pp. 972-977). Bangkok, Thailand.

Wongwatcharaphon, K., Tongtem, P., & Jugjai, S. 2013. Numerical and experimental study of late mixing porous burner. *Journal of the Energy Institute, 86*(1), 15-23.

Wood, S., & Harris, A. T. (2008). Porous burners for lean-burn applications, Combustion of hydrocarbon fuels within porous inert media, *Progress in Energy and Combustion Science, 34*, 667-684.

Yoshizawa, Y., Asaki, K., & Echigo, R. (1988). Analytical study of the structure of radiation controlled flame. *International Journal of Heat and Mass Transfer, 31*, 311-319.